Identification of Circumferential Regional Heterogeneity of Ascending Thoracic Aneurysmal Aorta by Biaxial Mechanical Testing

Marzio Di Giuseppe[1], Gioacchino Alotta[2], Valentina Agnese[3], Diego Bellavia[3], Giuseppe M Raffa[3], Valeria Vetri[4], Massimiliano Zingales[2], Salvatore Pasta[3,5], Michele Pilato[3]

[1] Promozione della Salute, Materno-Infantile, di Medicina Interna e Specialistica di Eccellenza "G. D'Alessandro", Piazza delle Cliniche, n.2, 90128, University of Palermo, Palermo, Italy

[2] Department of Engineering, Viale delle Scienze, Ed.8, 90128, University of Palermo, Palermo, Italy

[3] Department for the Treatment and Study of Cardiothoracic Diseases and Cardiothoracic Transplantation, IRCCS-ISMETT, Via Tricomi n.5, 90127, Palermo, Italy

[4] Dipartimento di Fisica e Chimica – Emilio Segrè, Viale delle Scienze, Ed. 17,90128, University of Palermo, Palermo, Italy

[5] Fondazione Ri.MED, Via Bandiera n.11, 90133, Palermo, Italy

Conflict of interest: none

[*] Corresponding author:
Salvatore Pasta, PhD
NSQ as Professor of Industrial Bioengineering,
Fondazione Ri.MED
Phone: +39 091 3815681
FAX: +39 091 3815682
e-mail: spasta@fondazionerimed.com

ABSTRACT

Ascending thoracic aortic aneurysm (ATAA) in patients with bicuspid aortic valve (BAV) can present an asymmetrical aortic dilatation compared with patients with tricuspid aortic valve (TAV). This pattern of aneurysm dilatation led us to hypothesize that biomechanical differences likely induced by regional heterogeneity of material properties can underlie the observed asymmetric enlargement discrepancies between BAV ATAA and TAV ATAA. This study aimed to characterize the mechanical properties and associated aortic tissue stiffness changes along the circumferential direction of aortic rings collected from surgically-repaired patients with ATAA. Biaxial material testing was performed on tissue specimens extrapolated from all aortic quadrants (i.e. anterior, posterior, major and minor curvature of the aorta), and then the tissue stiffness was quantified at both physiological and supra-physiological stress levels (i.e. 142kPa and 242kPa, respectively). Tissue stiffness revealed that the major curvature of BAV ATAA is statistically less stiff than the anterior quadrant (276.6±137.1kPa for BAV ATAA and 830.1±557.1kPa for BAV ATAA, p=0.024, at 142kPa) and to that of major curvature of TAV ATAA (276.6±137.0kPa for BAV ATAA and 733.2±391.1kPa for TAV ATAA, p=0.001, at 142 kPa), suggesting local weakening of bicuspid aortic wall. Multiphoton imaging revealed local changes on elastic fiber networks. The recovered material parameters for the Fung-type constitutive model are crucial for reliable stress predictions while the information on regional tissue stiffness changes are fundamental to develop risk stratification strategies not based on aortic size.

Keywords: ascending aortic aneurysm; bicuspid aortic valve, material parameters, biaxial testing, tissue stiffness

INTRODUCTION

Ascending thoracic aortic aneurysm (ATAA) is a life-threatening cardiovascular disease leading to weakening of the aortic wall and permanent dilation associated to high risk of adverse events [1]. ATAA affects approximately 10 out of 100,000 persons per year [2], with bicuspid aortic valve (BAV) patients having associated aortopathy on approximately 40% of bicuspid population [3]. The risk of complications such as aortic dissection and rupture are higher in BAV patients than that of patients with the morphological-normal tricuspid aortic valve (TAV) [4]. To avoid aortic complications, current clinical management of ATAA is based on strict monitoring of aneurysms size as well as elective repair when aortic diameter enlarges upon a critical size [5]. Aortic size is not a good predictor of ATAA failure, and this is known as the “size paradox” [6].

Aortic stiffness is associated with progressive aortic dilatation and aneurysm formation as shown by different imaging modalities [7, 8], computational analyses [9-11] and histological changes [12]. Higher aortic stiffness was associated with higher rates of surgical aortic replacement and aortic root dilation in children and young adults with connective tissue disorders [13]. In Marfan patients, aortic stiffness proved to have an important value in predicting progressive aortic dilatation [14]. A recent study of abdominal aortic aneurysms found that segmental stiffening of the aorta preceded aneurysm growth and introduced the concept that stiffening may act as an early mechanism triggering elastin breakdown and aneurysm growth [15]. However, aortic stiffness is not homogenous along the circumferential direction of the ascending aneurysmal aorta, thereby exposing local regions of the vessel at greater risk of complications than others. Alternative risk strategies, as opposed to the maximum aortic diameter criterion, are being developed by evaluating changes in the aortic stiffness of the ATAA wall [9, 16, 17]. These approaches rely on the utilize of computational tools to non-invasively estimate wall stress/strain using homogenous material properties along the circumferential direction of diseased aorta.

This study was undertaken to quantify the degree of regional heterogeneity of the ascending aneurysmal aorta as well as to determine differences of mechanical properties for their implementation on computational wall stress predictions. Specifically, equibiaxial mechanical testing was performed on tissue specimens extrapolated from aortic quadrants (i.e. anterior, posterior, major and minor curvature) of ATAA rings obtained from surgically-repaired patients with either BAV or TAV. The Fung-type constitutive equation was achieved for each aortic quadrant, and then the specimen tissue stiffness was derived at both physiological and supraphysiological stress levels to compare differences among groups.

METHODS

Study Population and Specimen Preparation

Aortic tissue samples were obtained from patients underwent repair of the aneurysmal ascending aorta at IRCCS ISMETT as part of their clinical care and not for the purpose of the study. All patients signed an informed consent before surgery, and the study was approved by the local ethical committee (IRRB/04/14). Indication for aortic surgery was based on aortic size measurement, predisposing risk factors, bicuspid aortopathy and familiarities. A total of 36 aortic segments (n.10 BAV ATAA and n.26 TAV ATAA) were analyzed by biaxial testing and grouped according to the aortic valve morphology (i.e. BAV vs TAV) as seen by computed-tomography (CT) imaging parallel to the aortic valve plane. After surgery, ATAA samples were cryopreserved in a calcium-free and glucose-free 0.9% physiological saline solution and stored at -80°C before material testing and multiphoton imaging. Along circumferential direction of ascending aorta, the harvested tissue ring was cut into squared specimens from each quadrant as a following: a) anterior, b) posterior, c) major curvature and d) minor curvature of the aorta (Figure 1). Thickness and dimensions of each squared sample were measured using a caliber

before material testing. Table 1 summarizes clinical demographics data and thickness measurements for each specimen.

Biaxial Testing

Experimentally-related material properties from aneurysm tissue samples collected were estimated by equibiaxial mechanical testing using an ElectroForce TestBench system (TA Instrument, Boston, MA). Square specimens (15x15mm) were anchored by sutures on specimen edge using small, surgical fishhooks. These sutures were attached to the four electromagnetic motors of the biaxial system, aligning circumferential and longitudinal edges with direction of stretching. Five black markers were placed on the side of intimal tissue surface to evaluate engineering strains along testing directions using a digital video extensometer placed perpendicularly to the testing area. During biaxial loading, the specimen was sub-merged in a bath with 0.9% physiologic saline solution under controlled temperature of 37^{o}C while a small preload (0.5 grams) was set prior to the displacement-driven testing protocol. A constant speed of 1mm/min was applied to each motor to stretch the specimen under equibiaxial condition. Two 200N load cells were used to record the force along material directions. Data analysis to obtain stress and strain were calculated as defined in the next section.

Data Analysis

From marker positions, the in-plane Green strain tensor was calculated as:

$$\boldsymbol{E} = \frac{1}{2}\left(\boldsymbol{F}^T\boldsymbol{F} - 1\right) \tag{1}$$

where **F** is the gradient deformation tensor. For in-plane biaxial stretching, the in plane Green strains are

$$E_{\theta\theta} = \frac{1}{2}\left(\lambda_{\theta}^2 - 1\right) \tag{2.a}$$

$$E_{\mathrm{LL}} = \frac{1}{2}\left(\lambda_{\mathrm{L}}^2 - 1\right) \tag{2.b}$$

where λ_θ and λ_L are the circumferential and longitudinal stretches in the deformed equilibrium configuration, respectively.

The first Piola–Kirchhoff stress tensor **P** was calculated from measured loads and initial specimen dimensions so that nonzero components of **P** are:

$$P_{\theta\theta} = \frac{f_\theta}{H X_{\mathrm{L}}} \tag{3.a}$$

$$P_{\mathrm{LL}} = \frac{f_{\mathrm{L}}}{H X_\theta} \tag{3.b}$$

where f_θ and f_{L} are the measured loads along each direction, X_θ and X_{L} are the unloaded specimen dimension along each direction, and H is the averaged specimen thickness in the unloaded reference configuration.

Constitutive Modeling

Soft tissues are primarily composed by water and have negligible permeability, resulting as an incompressible material. Blood vessels undergo finite deformations under normal and pathological conditions. For this reason, ATAA tissues can be considered elastic, homogenous, hyperelastic and incompressible, with the stress-strain material response mathematically described by a constitutive equation derived from scalar strain energy function W:

$$W = \frac{c}{2}(e^Q - 1) \tag{4}$$

with

$$Q \quad = (b_1 E_{\theta\theta}^2 + 2b_4 E_{LL} E_{\theta\theta} + b_2 E_{LL}^2) \tag{6}$$

where c is a material parameter $[\frac{N}{m^2}]$ and b_1,b_4,b_3 are dimensionless parameters.

The stress-strain data were fit to the following response functions, describing second Piola-Kirchoff stress tensors:

$$\boldsymbol{T}_{\theta\theta} = 2ce^{Q}(b_1 E_{\theta\theta} + b_4 E_{LL}) \quad (7.a)$$

$$\boldsymbol{T}_{LL} = 2ce^{Q}(b_4 E_{\theta\theta} + b_2 E_{LL}) \quad (7.b)$$

These response functions allow the interpolation of each stress component within the experimental strain range for $E_{\theta\theta}$ and E_{LL}. Fitting was performed with the nonlinear regression software package Hyperfit (v. 1.169, Brno, Czech Republic). For the Fung-exponential form, physically meaningful and plausible material parameters for the convergence of numerical solutions can be obtained by enforcing the convexity of the strain energy function and thus performing constrained minimization. For biaxial loading of soft tissue, strict convexity physically implies that the projections of the contour on the plane form a convex surface [18]. It can be shown that if c>0, then Eq.6 is likely convex if and only if b_1>0, b_2>0 and b_4>0

Multiphoton Imaging

For each aortic quadrant, square specimens (5x5mm) for multiphoton imaging investigation were cut next to specimens used for biomechanical testing. Then, tissue specimens were fixed in 4% paraformaldehyde for 2 hours, approximately and stored in PBS solution at 4^{o}C temperature prior imaging analysis. Samples were sealed in suitable chambered cover glasses. Three-dimensional (3D) images stacks were acquired at 1024×1024 pixel resolution using a Leica TCS SP5 confocal laser scanning microscope with a 40× oil objective (Leica Microsystems, Germany). The acquired image depth range was 20-60 μm with Z steps of 2 μm. The two-photon excitation (Spectra-Physics Mai-Tai Ti:Sa ultra-fast laser) was set at 880 nm.

Second Harmonic Generation (SHG) signal was detected in the range of 390-460 nm (green channel) while tissue autofluorescence in the range of 485-650 nm (red channel). Scanning frequency was 400 Hz, with each image resulting from the average of 5 acquisitions. Green channel signal was mainly attributed to collagen fibers in SHG while red signal channel was tissue auto fluorescence brighter signal for elastin fibers that is clearly distinguishable from background.

Statistics

Tissue stiffness defined as the first derivative of the stress-strain response at a given point was obtained at two stress levels for appropriate comparison. Specifically, physiological and supraphysiological tissue stiffnesses were evaluated at 143kPa and 242kPa, considering a systolic blood pressure of 120mmHg and a hypertensive blood pressure of 180mmHg, respectively. These stress levels were calculated based on the Laplace equation using average thickness and diameter of ascending aorta samples (see Table 1).

Rank Sum test was used to compare clinical demographic data and assess differences in the material properties between BAV ATAA and TAV ATAA as well as material directions (i.e., circumferential, CIRC, and longitudinal, LONG, directions). One-way ANOVA, followed by Holm-Sidak posthoc test for all pair-wise comparisons, was used to assess differences in the stiffness values computed for each quadrant at both physiological and supraphysiological stress levels. The association of tissue stiffness with aortic diameter and patient age was explored *via* Pearson's correlation. For the Fung-type constitutive model, the coefficient of determination (R^2) and the normalized-root-mean-square-error (NRMSE) were used as a measure for the "goodness of fit". Statistical analyses were performed using SigmaPlot (Systat Software Inc, San Jose, California), with statistical significance set to $p=0.05$ in all cases. Data are shown as Mean±SEM.

RESULTS

Table 1 summarizes patient demographics and thickness measurements of aortic tissue specimens cut from each aortic quadrant. The distribution of age in BAV ATAA differs statistically from that of TAV ATAA patients (64.6±9.7yrs for BAV ATAA vs 71.9±8.9yrs for TAV ATAA, p=0.037). There were no significant differences in the aortic diameter between BAV ATAA and TAV ATAA (50.7±5.3mm for BAV ATAA vs 55.9±7.5mm for TAV ATAA, p=0.054) as well as the specimen thickness among each aortic quadrant and among patient groups (2.1±0.4mm average thickness for BAV ATAA and 2.3±0.5mm average thickness for TAV ATAA, p=0.349).

Experimental raw data obtained from equibiaxial stretching of BAV ATAA and TAV ATAA tissue samples are reported for each region as stress-strain plots in CIRC and LONG directions as shown by Figure 2 and Figure A.1, respectively. Stress-strain profiles under equibiaxial loading exhibited a nonlinear and hyperelastic mechanical response, which is independent from aortic valve morphotype, aortic quadrant and loading direction. Stress-strain data were fit to the Fung-type constitutive equation, and average material coefficients obtained from the fitting optimization are reported in Table 2. Material parameters were successfully recovered upon 60% of Green strain. Fits provided values of coefficient of determination ranging between 0.83 and 0.99, thus suggesting a satisfactory fitting of equibiaxial stress-strain profiles.

For BAV ATAA and TAV ATAA, average tissue stiffnesses calculated as the mean values of all aortic quadrants at both 143 kPa and 242 kPa are shown by Figure 3. At both physiological and supraphysiological stress levels, there was no statistical difference on average stiffness of BAV ATAA as compared to that of TAV ATAA in either LONG (eg, 567.8±181.1kPa for BAV ATAA and 739.9±371.2kPa for TAV ATAA at 143kPa, p=0.176) and CIRC (eg, 660.4±369.9kPa for

BAV ATAA and 761.5±325.1kPa for TAV ATAA at 143kPa, p=0.427) directions of material stretching.

Regional heterogeneity of ATAA tissue stiffness revealed that the major curvature of the ascending aorta with BAV is statistically less stiff than that of TAV patients in the CIRC direction at both 143 kPa (276.6±137.0kPa for BAV ATAA and 733.2±391.1kPa for TAV ATAA, p=0.001) and 242 kPa (355.5±189.5kPa for BAV ATAA and 965.7±533.0kPa for TAV ATAA, p=0.001) as shown by Figure 4. We also found that the major curvature of BAV ATAA is less stiff than the anterior quadrant of the tissue specimen collected from the same patient at both 143kPa (276.6±137.1kPa for BAV ATAA and 830.1±557.1kPa for BAV ATAA, p=0.024) and 242kPa (355.5±189.5kPa for BAV ATAA and 1197.1±804.8kPa for BAV ATAA, p=0.017), suggesting local weakening of ATAA wall. There was no statistical difference in the mean values of tissue stiffness for other aortic quadrants.

Correlations of ATAA tissue stiffness with patient age and aortic valve diameter are shown by Figure 5. Correlations were evaluated at physiological and supraphysiological stress levels and, when observed, were statistically relevant at both levels. Aortic tissue stiffness value was positively correlated to the patient age of TAV ATAAs (R=0.492 and p=0.0106 at 143kPa), but not significantly for BAV ATAAs (R=0.102 and p=0.780 at 143kPa). Significant positive correlation was found between tissue stiffness and aortic diameter for BAV ATAAs (R=0.685 and p=0.0289 at 143kPa). A similar trend was observed between stiffness and aortic diameter for TAV ATAAs, although not statistically significant (R=0.182 and p=0.373 at 143kPa).

Figure 6 shows the overlap of about 50 μm depth multiphoton images for each quadrant in both BAV ATAA and TAV ATAA tissue sample. A representative 3D reconstruction and Z-axis stack images movies are reported in Video 1 and 2, respectively. The architecture of aneurysmal

aorta in either BAV or TAV is detected at the microscale and revealed that both elastin (red) and collagen (green) fibers are disorganized as compared to our previous investigation [19]. Elastin fibers appeared of the same thickness, being present both as thin straighter filaments and tick curly disorganized fibers. Differences in fiber length between BAV and TAV ATAA tissue samples cannot be assessed. For major, anterior and posterior quadrants, tissue samples of BAV ATAA highlighted elastin fibrils characterized by higher density, larger disorganization and straight bans as compared to that TAV-related samples showing collagen fiber fascicles organized along a preferential direction and thickness of 20 μm.

DISCUSSION

In this study, we examined mechanical properties of BAV ATAA and TAV ATAA tissue samples using planar equibiaxial material testing. Tissue behavior was quantified by tissue stiffness for all quadrants of aneurysmal aorta, and direct comparison was done to assess regional heterogeneity of biomechanical properties of diseased aorta along the circumferential direction. The most striking finding is that the major curvature of aneurysmal aorta from patients with BAV is weaker than that observed on the anterior region and to that of TAV patients in the same quadrant. This is likely a consequence of mechanical weakening characteristics of bicuspid aortopathy caused by diverse pathogenetic inferences.

Although the aortic size criterion can be adjusted to achieve higher patient specificity using the body surface area, the surgical dilemma on the optimal timing for elective repair of an ATAA still exists because fatal complications can occur at aortic diameters lower than that dictated by current clinical guidelines [7]. There is therefore a need to delineate additional metrics, not based on aortic size, to better identify the risk of ATAA failure. Indeed, the maximum aortic diameter as standard criterion for ATAAs is a surrogate geometric indicator of the imbalance between biomechanical stress and strength, which is what ultimately determines the rupture of

dilated ascending aortas. Although a biomechanical approach is far away from clinical application, findings on the strength of ATAAs as here presented do not only elucidate the mechanobiology of this deadly pathology but can also lead to better patient stratification criteria for surgery.

There are two possible explanations for our findings: 1) the presence of the BAV-related morphology has led to hemodynamic disturbances locally increasing wall shear stress in the major curvature of the ascending aorta so that the prolonged exposure to aortic shear stress led to weakening of the aortic wall; 2) an inherent fiber defect due to genetic causes of bicuspid aortopathy has disorganized fiber architecture of extracellular matrix (as partially confirmed by multiphoton imaging) to determine aortic wall weakening and dilatation. While the first evidence is supported by the fact that bulged aortic dilatations are commonly seen in BAV patients at the time of surgery or CT imaging [20, 21], the second comment rises by studies documenting increased proteolytic activity in surgically resected BAV tissues showing the presence of thin, fragmented elastin fibers, reduced fibrillin-1 content, and decreased types I and III collagen in the major curvature of aneurysmal ascending aorta [22, 23]. Matrix metalloproteases (MMP) are also differentially expressed across different aortic sites in BAV patients, with high concentrations of MMP-2 and associated tissue inhibitor (TIMP-3) in the concavity of ascending aorta [24]. These differences were also documented by tissue changes on microRNA expression when comparing convex and concave portions of dilated aortas in BAV patients [25]. In contrast, several hemodynamic studies using 4D Flow MRI [26, 27] or computational analyses [28-31] have elucidated that distinct aortic cusp fusion patterns of BAV phenotypes result in specific orientations of eccentric flow jets which in turn may lead to regionally-located distributions of aortic shear stress, leading to adverse vascular remodeling and weakening of the aortic wall. These clinical evidences and histological changes are used to alternatively support the dichotomy between hemodynamic-mediated aneurysm progression versus the

genetic theory of aortic dilatation. To our knowledge, this is the first study reporting the heterogeneity of aortic tissue stiffness of ATAAs with either BAV or TAV. Although several speculations are proposed, further studies are need to univocally asses the main cause of tissue stiffness changes. Computational simulations based on virtual anatomic reconstructions of the ATAA geometry could potential reveals whether the major curvature of aneurysmal aorta of our BAV patients was really exposed to high shear stress; however, only four patients underwent CT imaging in our hospital while others arrived from external centers. Familiarity for ATAA was reported by six patients but a genetic investigation was not undertaken in this study.

The heterogeneity of the ascending aorta is at two levels, that due to the layering along the tissue thickness (ie, intima, media and adventitia) and that due to each layer along the circumferential regions of the vessel (ie, anterior, posterior, major and minor curvature). Holzapfel et al [32] reported different material properties and fiber angle for each aortic layer while Deveja et al [33] revealed that layer-specific extensibility was significantly greater in BAV ATAAs than in TAV ATAAs, unaccounted by elastin/collagen content changes. On artificially dissected aortic tissue specimens, we found that the inner layers ruptured earlier then the outer layer [34], and then observed correlation with collagen fiber architecture assessed by multiphoton imaging [35]. Although multiphoton shown regional changes in the fiber architecture of each quadrant [36], several studies using uniaxial tensile testing did not highlight any regional changes in the elastic modulus and stress values at rupture of the ATAA wall, but observed stiffness differences according to material testing direction [33, 37, 38]. Comparison with our result is not straightforward, as we performed equibiaxial testing that is more appropriate for the membrane-like ascending aorta with respect to uniaxial testing. In general, if the major curvature of aneurysmal aorta is weaker than other quadrants, this is likely at high risk of complications. Regional variations of constitutive properties make also sense as they can be related to local tissue adaptation through growth and remodeling.

The fidelity of wall stress predictions is affected by changes on constitutive material parameters and fiber architecture along the circumferential direction of the aorta. In our opinion, regional heterogeneity has to be considered in patient-specific computational analyses of ATAA mechanics because, according to equilibrium equation, the analysis of the wall stress in a curved ascending aorta indicates that the circumferential stress is much larger on the lower curvature of the aortic wall than that of the greater curvature where rupture/dissection are clinically seen. If not considered, this geometrical nature of the aneurysmal ascending aorta can therefore lead to erroneous predictions of computational wall stress even if we account for layer heterogeneity by using a fiber-reinforced material model as that proposed by Gasser [39]. The difference in the material parameters here reported can be used in rotationally symmetric dispersion model as that proposed by Holzapfel et al [40] to account for regional heterogeneity and associated fiber changes.

Another relevant finding is the corroboration of tissue stiffness increase with patient age. Indeed, a loss of arterial elasticity is common in ascending aortic aneurysms as documented by two-dimensional speckle-tracking echocardiography [7], medical images analysis of dynamic CT images [10, 11] or bulge-inflation experimental testing [17]. These studies documented not appreciable variation on ATAA tissue stiffness between BAV and TAV patients, suggesting that clinical management of BAV patients should be similar to that of general tricuspid population. Strain-based rupture estimation relying on the imbalance between aortic strain and strength at rupture and have demonstrated that that only a stiffer dilated aorta with increased blood pressure could significantly increase the risk of rupture [16, 17]. Less stiff aortic regions are however not necessary at greatest risk of failure because of variability on the aortic wall strength (ie, the ability of the material to withstand a loading condition). The aortic strength is therefore

an important determinant of ATAA failure and can be only estimated by *ex-vivo* mechanical testing.

This study has some limitations. Biaxial mechanical properties were not investigated for the non-aneurysmal aorta because of difficulties on collecting aortic tissues from organ donors or heart transplant recipients. The study of Azadani et al. [41] document Fung-type material coefficient and tissue stiffness changes on healthy aortas, although with no details on regional heterogeneity. The biaxial mechanical protocol was extended to an equibiaxial loading condition whereas the full anisotropic behavior of the aorta can be captured varying the stress ratio along material stretching directions. Lastly, tissue stress levels were estimated based on the Laplace equation, which relies on cylindrical geometry rather than true ATAA geometry to determine wall stress. More accurate stress levels can be obtained by computational studies incorporating patient-specific ATAA geometries. A larger sample size for BAV study group would be ideal to confirm observations, although statistical power was found relevant.

CONCLUSION

We concluded that tissue stiffness determined from stress-strain curves under equibiaxial loading is heterogeneous among aortic quadrants in ATAAs, with the major curvature of aneurysmal aorta of BAV patients weaker than that observed on the anterior region and to that of TAV patients in the same quadrant. The recovered material parameters for the Fung-type constitutive model are crucial for reliable stress predictions and for the development of risk stratification strategies not based on aortic size.

ACKNOWLEDGMENTS

We thank Dr. Pietro Tagliareni for aortic specimen acquisition. This work was supported by a “Ricerca Finalizzata” grant from the Italian Ministry of Health (GR-2011-02348129) to Salvatore

Pasta, by a grant from Fondazione RiMED to Salvatore Pasta, and by grant from PON FSE-FESR Ricerca Innovazione 2014-2020 to Marzio Di Giuseppe. This study was undertaken at BNM2-Lab of ATeN Center led by Massimiliano Zingales.

REFERENCES

[1] Elefteriades JA, Farkas EA. Thoracic aortic aneurysm clinically pertinent controversies and uncertainties. J Am Coll Cardiol. 2010;55:841-57.

[2] Coady MA, Rizzo JA, Goldstein LJ, Elefteriades JA. Natural history, pathogenesis, and etiology of thoracic aortic aneurysms and dissections. Cardiol Clin. 1999;17:615-35; vii.

[3] Verma S, Siu SC. Aortic dilatation in patients with bicuspid aortic valve. N Engl J Med. 2014;370:1920-9.

[4] Januzzi JL, Isselbacher EM, Fattori R, Cooper JV, Smith DE, Fang J, et al. Characterizing the young patient with aortic dissection: results from the International Registry of Aortic Dissection (IRAD). J Am Coll Cardiol. 2004;43:665-9.

[5] Borger MA, Fedak PWM, Stephens EH, Gleason TG, Girdauskas E, Ikonomidis JS, et al. The American Association for Thoracic Surgery consensus guidelines on bicuspid aortic valve-related aortopathy: Full online-only version. J Thorac Cardiovasc Surg. 2018;156:e41-e74.

[6] Pape LA, Tsai TT, Isselbacher EM, Oh JK, O'Gara PT, Evangelista A, et al. Aortic diameter >= 5.5 cm is not a good predictor of type A aortic dissection - Observations from the international registry of acute aortic dissection (IRAD). Circulation. 2007;116:1120-7.

[7] Teixeira R, Moreira N, Baptista R, Barbosa A, Martins R, Castro G, et al. Circumferential ascending aortic strain and aortic stenosis. Eur Heart J Cardiovasc Imaging. 2013;14:631-41.

[8] Longobardo L, Carerj ML, Pizzino G, Bitto A, Piccione MC, Zucco M, et al. Impairment of elastic properties of the aorta in bicuspid aortic valve: relationship between biomolecular and aortic strain patterns. Eur Heart J Cardiovasc Imaging. 2018;19:879-87.

[9] Farzaneh S, Trabelsi O, Avril S. Inverse identification of local stiffness across ascending thoracic aortic aneurysms. Biomech Model Mechanobiol. 2018.

[10] Pasta S, Agnese V, Di Giuseppe M, Gentile G, Raffa GM, Bellavia D, et al. In Vivo Strain Analysis of Dilated Ascending Thoracic Aorta by ECG-Gated CT Angiographic Imaging. Ann Biomed Eng. 2017.

[11] Martin C, Sun W, Primiano C, McKay R, Elefteriades J. Age-dependent ascending aorta mechanics assessed through multiphase CT. Ann Biomed Eng. 2013;41:2565-74.

[12] Selvin E, Najjar SS, Cornish TC, Halushka MK. A comprehensive histopathological evaluation of vascular medial fibrosis: insights into the pathophysiology of arterial stiffening. Atherosclerosis. 2010;208:69-74.

[13] Prakash A, Adlakha H, Rabideau N, Hass CJ, Morris SA, Geva T, et al. Segmental Aortic Stiffness in Children and Young Adults With Connective Tissue Disorders: Relationships With Age, Aortic Size, Rate of Dilation, and Surgical Root Replacement. Circulation. 2015;132:595-602.

[14] Sulejmani F, Pokutta-Paskaleva A, Ziganshin B, Leshnower B, Iannucci G, Elefteriades J, et al. Biomechanical properties of the thoracic aorta in Marfan patients. Annals of cardiothoracic surgery. 2017;6:610-24.

[15] Raaz U, Zollner AM, Schellinger IN, Toh R, Nakagami F, Brandt M, et al. Segmental aortic stiffening contributes to experimental abdominal aortic aneurysm development. Circulation. 2015;131:1783-95.

[16] Martin C, Sun W, Pham T, Elefteriades J. Predictive biomechanical analysis of ascending aortic aneurysm rupture potential. Acta Biomater. 2013;9:9392-400.

[17] Duprey A, Trabelsi O, Vola M, Favre JP, Avril S. Biaxial rupture properties of ascending thoracic aortic aneurysms. Acta Biomater. 2016;42:273-85.

[18] Holzapfel GA, Gasser TC, Ogden RW. A New Constitutive Framework for Arterial Wall Mechanics and a Comparative Study of Material Models. Journal of elasticity and the physical science of solids. 2000;61:1-48.

[19] Pasta S, Phillippi JA, Tsamis A, D'Amore A, Raffa GM, Pilato M, et al. Constitutive modeling of ascending thoracic aortic aneurysms using microstructural parameters. Med Eng Phys. 2016;38:121-30.

[20] Hope MD, Hope TA, Crook SE, Ordovas KG, Urbania TH, Alley MT, et al. 4D flow CMR in assessment of valve-related ascending aortic disease. JACC Cardiovasc Imaging. 2011;4:781-7.

[21] Hope MD, Hope TA, Meadows AK, Ordovas KG, Urbania TH, Alley MT, et al. Bicuspid Aortic Valve: Four-dimensional MR Evaluation of Ascending Aortic Systolic Flow Patterns. Radiology. 2010;255:53-61.

[22] Cotrufo M, Della Corte A, De Santo LS, Quarto C, De Feo M, Romano G, et al. Different patterns of extracellular matrix protein expression in the convexity and the concavity of the dilated aorta with bicuspid aortic valve: preliminary results. J Thorac Cardiovasc Surg. 2005;130:504-11.

[23] Della Corte A, De Santo LS, Montagnani S, Quarto C, Romano G, Amarelli C, et al. Spatial patterns of matrix protein expression in dilated ascending aorta with aortic regurgitation: congenital bicuspid valve versus Marfan's syndrome. J Heart Valve Dis. 2006;15:20-7; discussion 7.

[24] Mohamed SA, Radtke A, Saraei R, Bullerdiek J, Sorani H, Nimzyk R, et al. Locally different endothelial nitric oxide synthase protein levels in ascending aortic aneurysms of bicuspid and tricuspid aortic valve. Cardiology research and practice. 2012;2012:165957.

[25] Albinsson S, Della Corte A, Alajbegovic A, Krawczyk KK, Bancone C, Galderisi U, et al. Patients with bicuspid and tricuspid aortic valve exhibit distinct regional microrna signatures in mildly dilated ascending aorta. Heart and Vessels. 2017;32:750-67.

[26] Barker AJ, Lanning C, Shandas R. Quantification of Hemodynamic Wall Shear Stress in Patients with Bicuspid Aortic Valve Using Phase-Contrast MRI. Annals of Biomedical Engineering. 2010;38:788-800.

[27] Mahadevia R, Barker AJ, Schnell S, Entezari P, Kansal P, Fedak PW, et al. Bicuspid aortic cusp fusion morphology alters aortic three-dimensional outflow patterns, wall shear stress, and expression of aortopathy. Circulation. 2014;129:673-82.

[28] Pasta S, Gentile G, Raffa GM, Bellavia D, Chiarello G, Liotta R, et al. In Silico Shear and Intramural Stresses are Linked to Aortic Valve Morphology in Dilated Ascending Aorta. Eur J Vasc Endovasc Surg. 2017;(in press).

[29] Rinaudo A, Pasta S. Regional variation of wall shear stress in ascending thoracic aortic aneurysms. Proceedings of the Institution of Mechanical Engineers Part H, Journal of engineering in medicine. 2014;228:627-38.

[30] Lee JJ, D'Ancona G, Amaducci A, Follis F, Pilato M, Pasta S. Role of computational modeling in thoracic aortic pathology: a review. J Card Surg. 2014;29:653-62.

[31] D'Ancona G, Amaducci A, Rinaudo A, Pasta S, Follis F, Pilato M, et al. Hemodynamic Predictors of a Penetrating Atherosclerotic Ulcer Rupture using Fluid-Structure Interaction Analysis ICVTS. 2013;17:576-8.

[32] Holzapfel GA, Sommer G, Auer M, Regitnig P, Ogden RW. Layer-specific 3D residual deformations of human aortas with non-atherosclerotic intimal thickening. Ann Biomed Eng. 2007;35:530-45.

[33] Deveja RP, Iliopoulos DC, Kritharis EP, Angouras DC, Sfyris D, Papadodima SA, et al. Effect of Aneurysm and Bicuspid Aortic Valve on Layer-Specific Ascending Aorta Mechanics. Ann Thorac Surg. 2018;106:1692-701.

[34] Pasta S, Phillippi JA, Gleason TG, Vorp DA. Effect of aneurysm on the mechanical dissection properties of the human ascending thoracic aorta. J Thorac Cardiovasc Surg. 2012;143:460-7.

[35] Tsamis A, Phillippi JA, Koch RG, Pasta S, D'Amore A, Watkins SC, et al. Fiber micro-architecture in the longitudinal-radial and circumferential-radial planes of ascending thoracic aortic aneurysm media. J Biomech. 2013;46:2787–94.

[36] Tsamis A, Phillippi JA, Koch RG, Chan PG, Krawiec JT, D'Amore A, et al. Extracellular matrix fiber microarchitecture is region-specific in bicuspid aortic valve-associated ascending aortopathy. J Thorac Cardiovasc Surg. 2016.

[37] Iliopoulos DC, Deveja RP, Kritharis EP, Perrea D, Sionis GD, Toutouzas K, et al. Regional and directional variations in the mechanical properties of ascending thoracic aortic aneurysms. Medical Engineering & Physics. 2009;31:1-9.

[38] Sokolis DP, Kritharis EP, Iliopoulos DC. Effect of layer heterogeneity on the biomechanical properties of ascending thoracic aortic aneurysms. Medical & Biological Engineering & Computing. 2012;50:1227-37.

[39] Gasser CT, Ogden RW, Holzapfel GA. Hyperelastic modelling of arterial layers with distributed collagen fibre orientations. J R Soc Interface 2006;3:15-35.

[40] Holzapfel GA, Niestrawska JA, Ogden RW, Reinisch AJ, Schriefl AJ. Modelling non-symmetric collagen fibre dispersion in arterial walls. J R Soc Interface. 2015;12.

[41] Azadani AN, Chitsaz S, Mannion A, Mookhoek A, Wisneski A, Guccione JM, et al. Biomechanical properties of human ascending thoracic aortic aneurysms. Ann Thorac Surg. 2013;96:50-8.

Figure Legends

Figure 1: (A) Equibiaxial testing device; (B and C) Picture of an ATAA sample just after collection during aneurysm surgical repair: the anterior, posterior, major curvature and minor curvature regions are shown in boxes; tissue specimens were harvested from these quadrants for biomechanical testing.

Figure 2: Equibiaxial raw stress-strain data from (A) BAV ATAA and (B) TAV ATAA specimens in the CIRC direction from the anterior, posterior, major curvature and minor curvature regions; each ID number represents the experimental raw data obtained from different patients.

Figure 3: Average stiffness values of BAV ATAA and TAV ATAA specimens at 143kPa (black bar) and 242 kPa (white bar) in (A) LONG and (B) CIRC directions.

Figure 4: Comparisons of average tissue stiffness of BAV ATAAs and TAV ATAAs at (A) 143kPa in LONG direction; (B) 143kPa in CIRC direction; (C) 242kPa in LONG direction; (D) 242kPa in CIRC direction.

Figure 5: (A) Correlation between stiffness and patient age for BAV ATAAs at 143kPa (solid circles) and 242kPa (solid triangles); (B) correlation between stiffness and aneurysm diameter for BAV ATAAs at 143kPa and 242kPa; (C) correlation between stiffness and patient age for TAV ATAAs at 143kPa and 242kPa; (D) correlation between stiffness and aneurysm diameter for TAV ATAAs at 143kPa and 242kPa.

Figure 6: Representative multiphoton microscopy measurements of BAV ATAA and TAV ATAA from anterior, posterior, major curvature and minor curvature (thickness of 50 μm); overlap of z-stack is reported; images acquired under laser excitation of λ_{exc}= 880 nm and SHG signal of collagen fiber in the range of 390-460 nm (green channel) and tissue autofluorescence in the range 485-650 nm (red channel) with elastin fibers clearly distinguishable from higher intensity and morphology.

Video 1: representative 3D reconstruction of a stack images for the anterior quadrant of a TAV ATAA tissue sample from patient ID.8

Video 2: Z-axis stack movies showing the overlaid images of the anterior quadrant of a TAV ATAA tissue sample from patient ID.8

Figure A.1: Equibiaxial raw stress-strain data from (A) BAV ATAA and (B) TAV ATAA specimens in the LONG direction from the anterior, posterior, major curvature and minor curvature regions; each ID number represents the experimental raw data obtained from a different patient.

Table 1: Demographic data and measurements of thickness along the circumferential direction of the ATAA

ID	Sex/Age/Valve	Diameter (mm)	Thickness Posterior (mm)	Thickness Major (mm)	Thickness Minor (mm)	Thickness Anterior (mm)
1	M/72/BAV	54	2.1	2.1	2.1	2.1
2	F/74/TAV	53	2.1	2.1	2.1	2.1
3	M/57/BAV	43	2.2	2.2	2.2	2.2
4	F/65/TAV	56	1.8	1.8	1.8	1.8
5	M/73/TAV	49	3.6	4.0	3.6	5.6
6	M/65/BAV	40	2.2	2.2	2.2	2.1
7	M/70/TAV	54	2.3	2.4	2.4	2.5
8	F/76/TAV	59	2.3	2.4	2.4	2.5
9	F/55/TAV	50	2.3	2.4	2.4	2.5
10	M/69/TAV	59	2.6	2.6	2.6	2.6
11	M/58/TAV	55	2.0	2.0	1.9	1.9
12	M/68/BAV	49	1.7	1.8	1.9	1.8
13	M/81/TAV	74	1.7	1.7	1.9	1.8
14	M/69/BAV	52	2.5	2.5	2.5	-
15	M/66/TAV	61	2.8	2.8	-	2.8
16	M/78/TAV	47	2.3	2.1	-	2.2
17	M/78/BAV	57	2.2	2.2	2.2	2.1
18	F/46/BAV	53	2.2	2.2	2.2	2.1
19	M/54/BAV	53	1.4	1.4	1.5	1.4
20	M/69/TAV	60	2.2	2.2	-	2.2
21	F/68/BAV	55	2.2	2.2	2.2	2.1
22	F/66/TAV	52	-	2.5	-	2.3
23	M/76/TAV	55	1.8	2.2	2.3	2.0
24	M/78/TAV	53	2.8	3.3	3.2	3.5
25	M/80/TAV	56	2.8	3.0	3.0	2.3
26	F/77/TAV	60	2.0	2.0	-	2.0
27	M/79/TAV	46	1.9	2.1	2.0	1.9
28	F/79/TAV	49	2.0	2.0	1.8	2.0
29	M/86/TAV	59	2.0	2.5	2.0	2.5
30	M/71/BAV	51	2.8	3.0	3.0	2.9
31	F/81/TAV	52	3.0	3.0	-	3.0
32	F/79/TAV	53	2.5	2.5	2.3	2.5
33	F/59/TAV	54	2.0	2.0	2.0	2.5
34	F/81/TAV	54	2.0	2.0	2.0	2.0
35	M/55/TAV	53	-	3.0	2.8	3.0
36	M/60/TAV	81	-	2.0	3.0	3.0
	69.9±9.6	54.5±7.3	2.24±0.44	2.34±0.50	2.32±0.47	2.39±0.71

Table 2: Constitutive material parameters of Fung-type material model resulting from the fitting of experimental stress-strain response

	c (kPa)	b1	b2	b4	R^2	NRMSE
BAV						
Major	46.8 ± 74.2	27.2 ± 43.9	12.5 ± 24.1	-2.2 ± 14.9	0.98-0.99	0.01-0.17
Minor	17.4 ± 12.3	3.3 ± 4.8	0.7 ± 1.8	4.3 ± 10.1	0.94-0.99	0.02-0.51
Posterior	27.2 ± 19.3	20.7 ± 44.5	5.7 ± 14.9	-2.3 ± 2.7	0.86-0.99	0.01-0.36
Anterior	42.6 ± 58.5	4.2 ± 4.5	6.4 ± 16.6	-0.1 ± 2.6	0.94-0.99	0.01-0.31
TAV						
Major	34.6 ± 30.3	19.3 ± 46.9	6.4 ± 13.7	1.8 ± 4.2	0.91-0.99	0.01-0.62
Minor	79.4 ± 142.3	21.6 ± 28.1	14.4 ± 19.8	23.8 ± 83.3	0.88-0.99	0.02-0.35
Posterior	73.5 ± 115.9	19.4 ± 30.7	12.0 ± 22.2	1.6 ± 5.1	0.88-0.99	0.02-0.37
Anterior	42.0 ± 67.6	29.9 ± 45.0	12.8 ± 33.4	1.5 ± 4.8	0.83-0.99	0.03-0.74

Figure 1

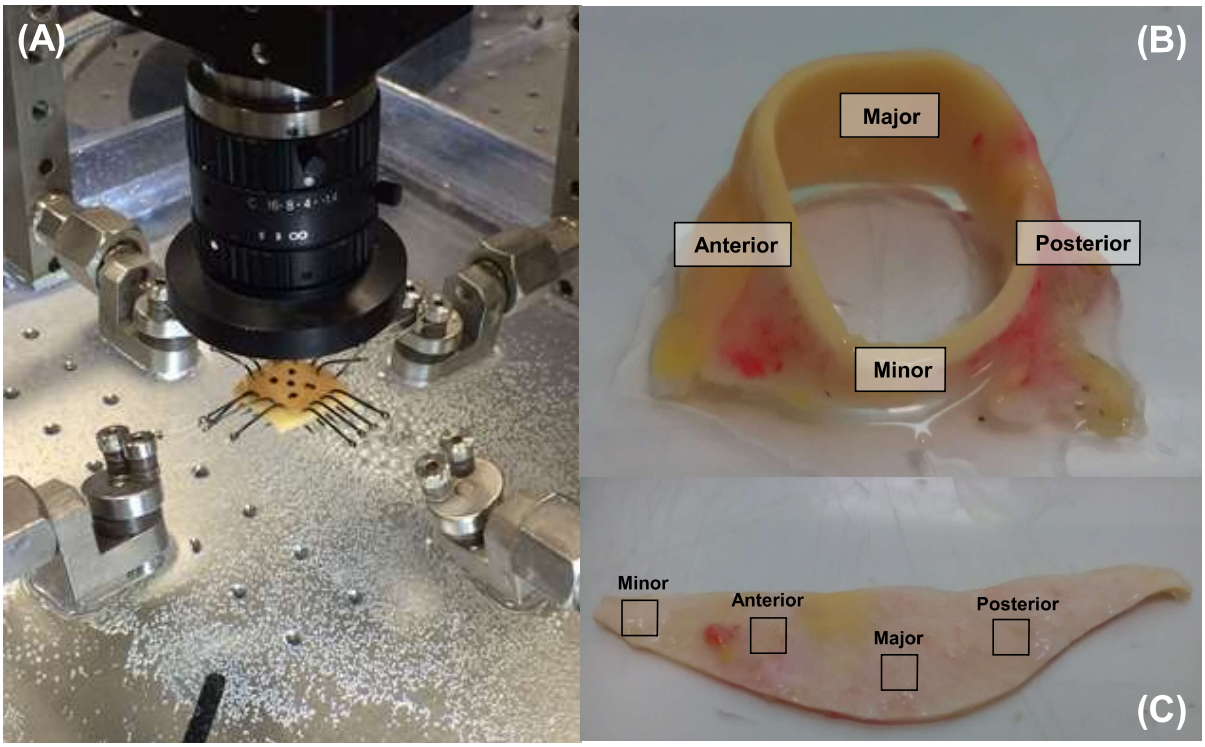
(A)
(B)
Major
Anterior
Posterior
Minor
Minor
Anterior
Major
Posterior
(C)

Figure 2

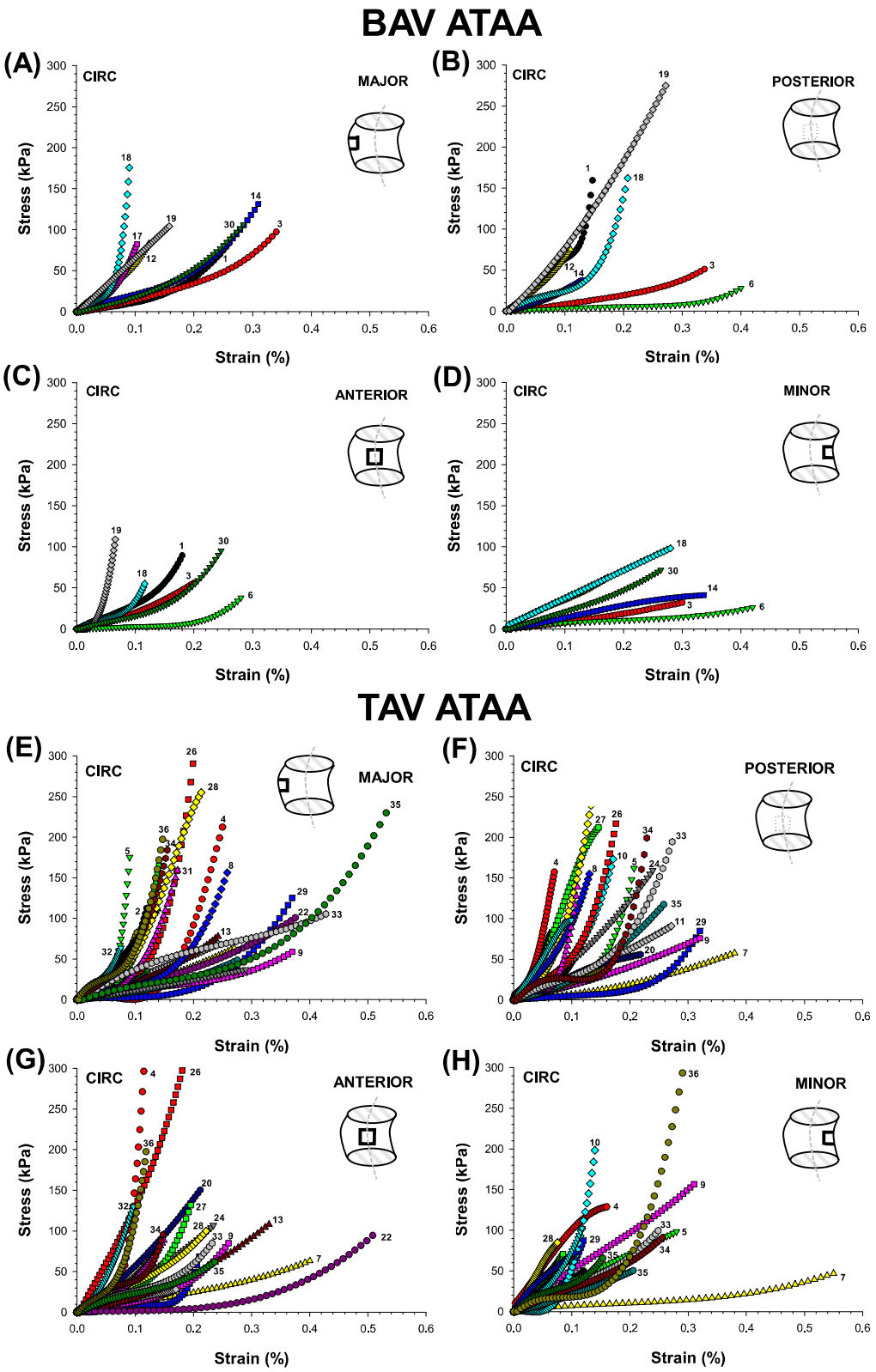
BAV ATAA
(A)
CIRC
MAJOR
(B)
CIRC
POSTERIOR
(C)
CIRC
ANTERIOR
(D)
CIRC
MINOR
TAV ATAA
(E)
CIRC
MAJOR
(F)
CIRC
POSTERIOR
(G)
CIRC
ANTERIOR
(H)
CIRC
MINOR
Stress (kPa)
Strain (%)

Figure 3

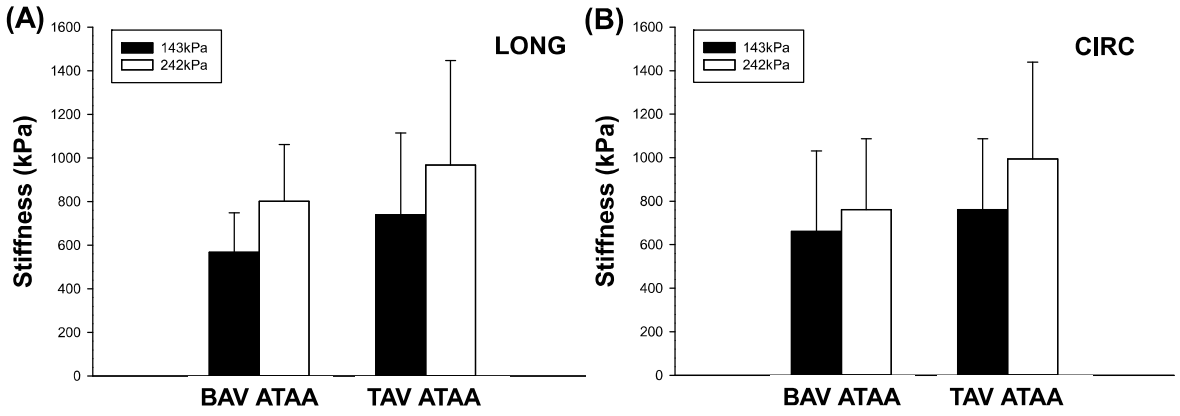
(A)
LONG
143kPa
242kPa
Stiffness (kPa)
1600
1400
1200
1000
800
600
400
200
0
BAV ATAA
TAV ATAA
(B)
CIRC
143kPa
242kPa
Stiffness (kPa)
BAV ATAA
TAV ATAA

Figure 4

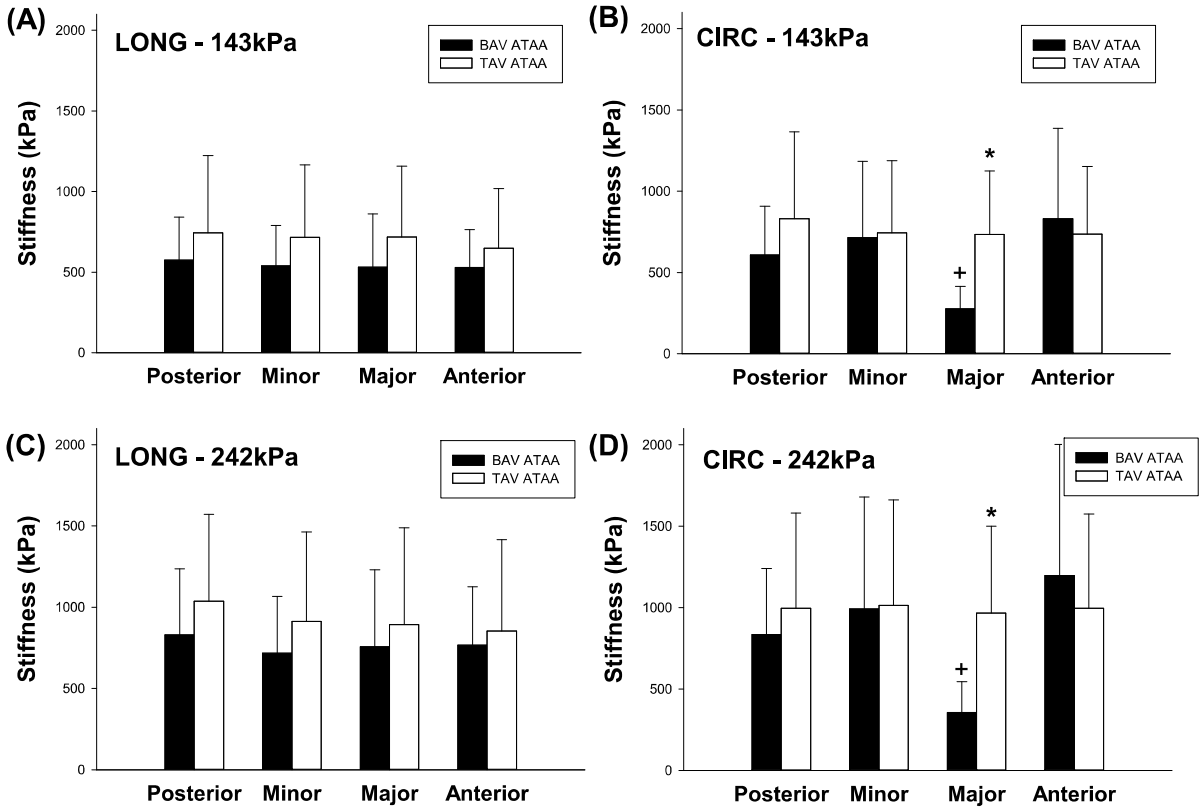
(A)
LONG - 143kPa
BAV ATAA
TAV ATAA
Stiffness (kPa)
2000
1500
1000
500
0
Posterior
Minor
Major
Anterior
(B)
CIRC - 143kPa
BAV ATAA
TAV ATAA
Stiffness (kPa)
*
+
Posterior
Minor
Major
Anterior
(C)
LONG - 242kPa
BAV ATAA
TAV ATAA
Stiffness (kPa)
Posterior
Minor
Major
Anterior
(D)
CIRC - 242kPa
BAV ATAA
TAV ATAA
Stiffness (kPa)
*
+
Posterior
Minor
Major
Anterior

Figure 5

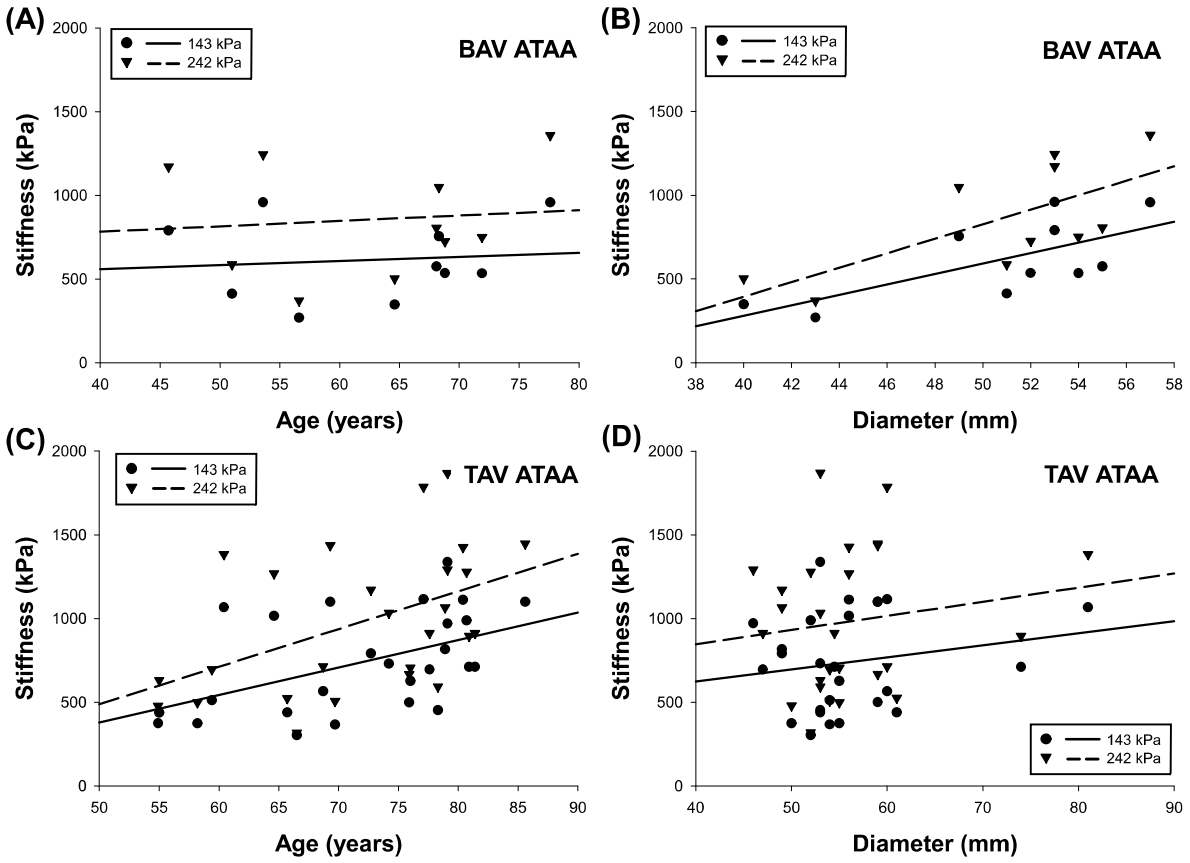
(A)
BAV ATAA
143 kPa
242 kPa
Stiffness (kPa)
Age (years)
(B)
BAV ATAA
Diameter (mm)
(C)
TAV ATAA
(D)
TAV ATAA

Figure 6

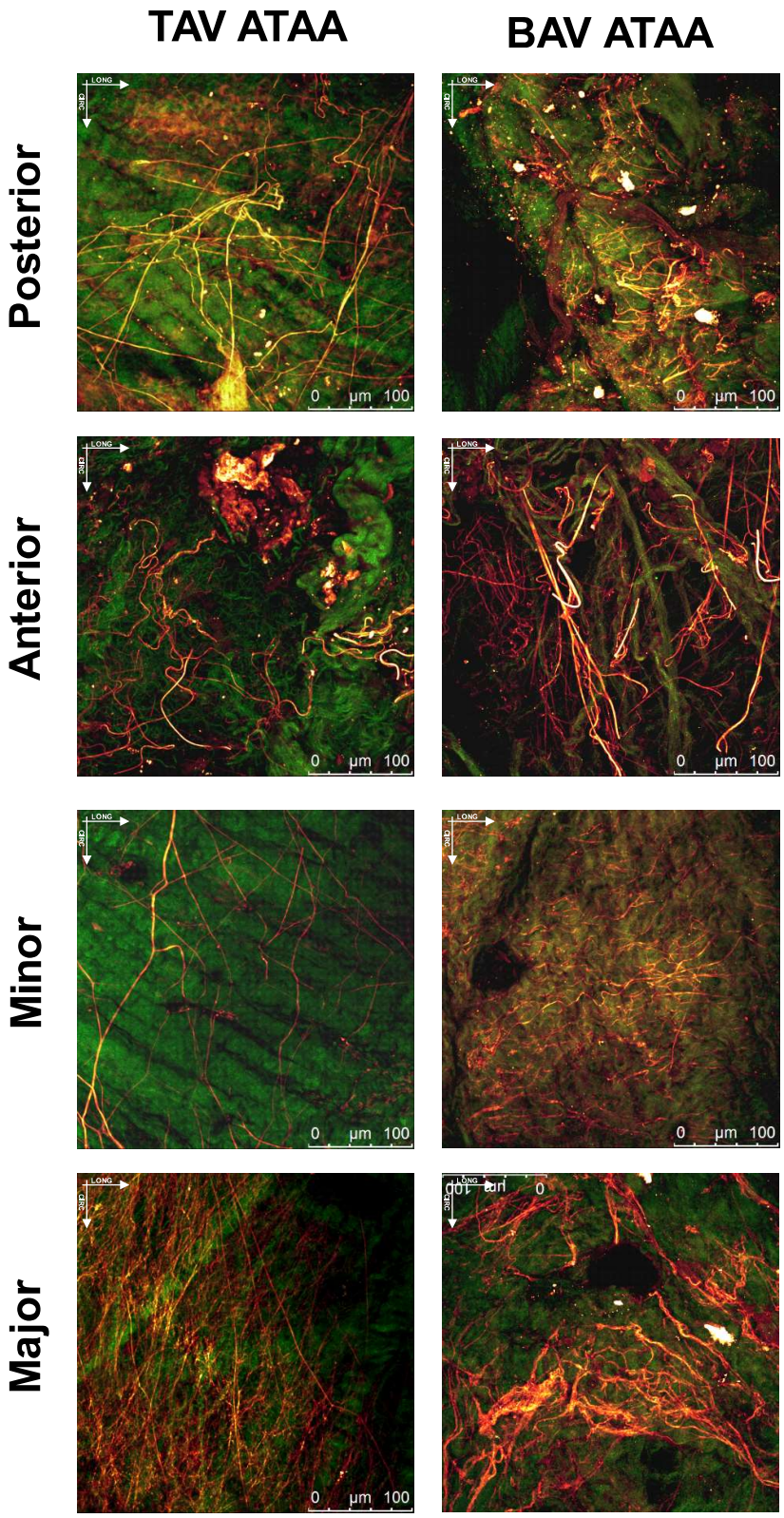
TAV ATAA
BAV ATAA
Posterior
Anterior
Minor
Major
LONG
CIRC
0 µm 100

Figure A.1

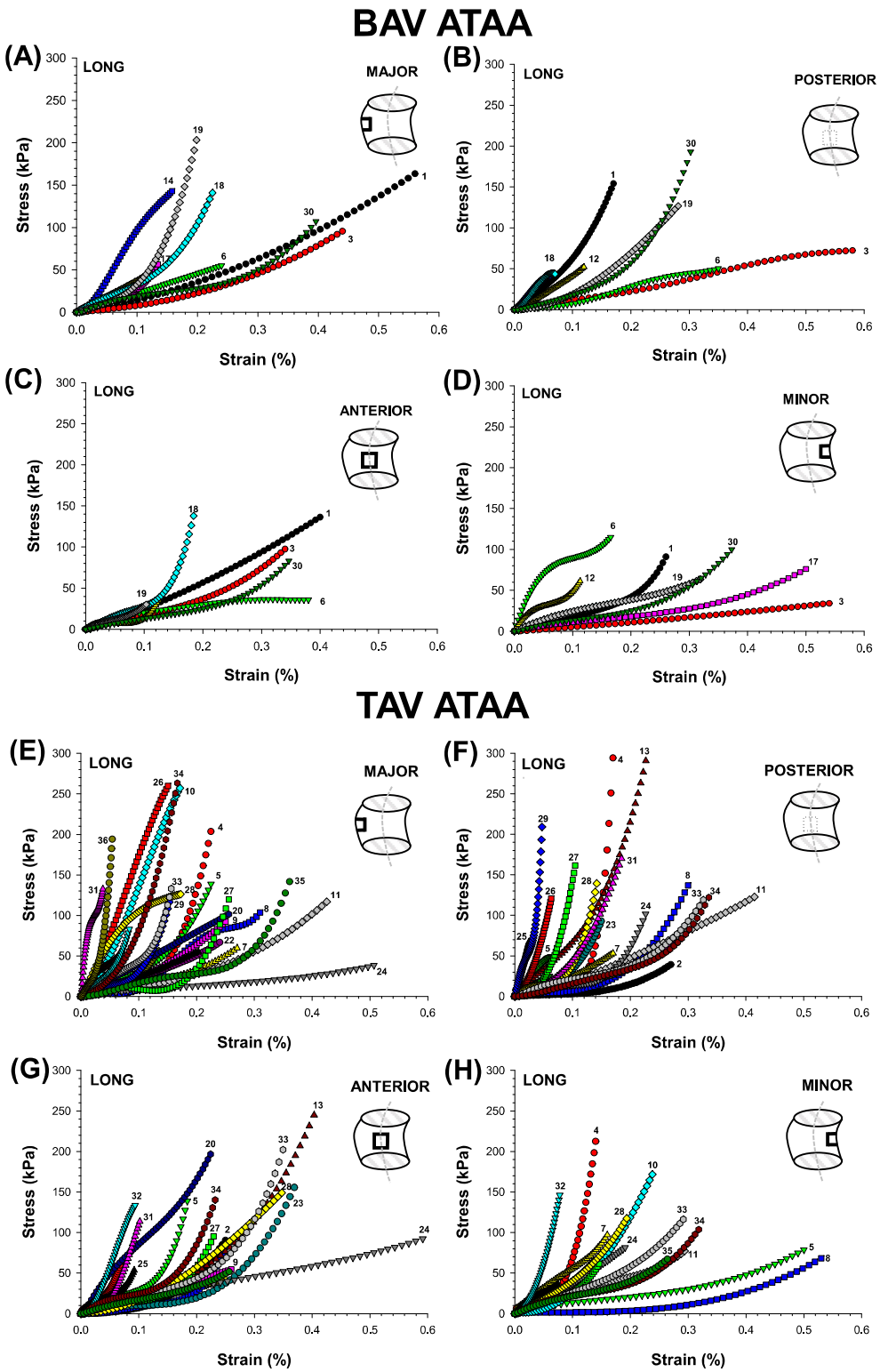
BAV ATAA
(A)
LONG
MAJOR
(B)
LONG
POSTERIOR
(C)
LONG
ANTERIOR
(D)
LONG
MINOR
TAV ATAA
(E)
LONG
MAJOR
(F)
LONG
POSTERIOR
(G)
LONG
ANTERIOR
(H)
LONG
MINOR
Stress (kPa)
Strain (%)